Acoustic Localization of an Intruder in a Strongly Scattering Medium

S. van den Wildenberg,[1,2,*] X. Jia,[3,4,†] J.L. Gennisson,[5] and A. Tourin[3]

[1] *CNRS, IRD, OPGC, Laboratoire Magmas et Volcans, Université Clermont Auvergne, Clermont-Ferrand F-63000, France*

[2] *CNRS/IN2P3, Laboratoire de Physique de Clermont, Université Clermont Auvergne, Clermont-Ferrand F-63000, France*

[3] *ESPCI Paris, PSL University, CNRS, Institut Langevin, Paris 75005, France*

[4] *Université Gustave Eiffel, Marne-la-Vallée 77454, France*

[5] *CEA, CNRS, Inserm, BioMaps, Université Paris-Saclay, Orsay 91401, France*

(Received 27 July 2022; revised 31 October 2022; accepted 16 November 2022; published 30 December 2022)

Localizing an intruder submerged in a strongly scattering medium, such as a dense granular suspension, is a practical challenge. Here we extract the coherent ultrasonic echo from a steel ball submerged in a dense glass-bead packing saturated by water, by using a standard single-element ultrasonic transducer thanks to a configuration averaging process. Different configurations of the granular packing are created by the nonaffine motion of the beads with a mixing blade, akin to the Brownian motion, in the vicinity of the intruder. We investigate the efficiency of this process to reduce the so-called material noise from multiply scattered ultrasound, as a function of the configuration number, the shear rate and the blade-intruder distance. Nonaffine motions of the beads in the shear zone induced by the blade are then analyzed on the basis of a split-bottom rotating shear cell. This method helps to develop not only ultrasonic imaging tools of buried objects in turbid marine sediments, but also the local rheology based on a ball falling monitored by ultrasonic tracking.

DOI: 10.1103/PhysRevApplied.18.064097

I. INTRODUCTION

Dense suspensions of small rigid particles in a Newtonian liquid are involved in many applications and geological processes such as mudflows and underwater avalanches [1,2]. Their rich dynamics depends to a large extent on the density mismatch between the suspending liquid and the solid particles [3–5]. Under gravity, the flow behavior of these suspensions can be roughly separated into two regimes [2,6]. In the fast-flow regime, momentum exchange takes place via a combination of collisions and enduring contacts and an inertial number I may be defined to characterize the local rapidity of the flow [7–9]. In the slow-flow regime, I is close to zero and the yields stress and momentum transfer are dominated by enduring frictional contacts. In this regime, the flow may tend to be localized, a phenomenon known as shear banding [10,11].

Rheometry is classically the tool of choice to characterize the flow properties of granular suspensions. However, it does not provide information on the local microstructural and/or flow heterogeneities. Therefore, rheological experiments have been combined with different imaging approaches [12], such as single scattering of light, neutron and x ray [13], magnetic resonance [14] or ultrafast ultrasonic imaging (velocimetry and elastography) [15–17]. Acoustic monitoring often presents the advantages of being fast and applicable in optically opaque media, such as three-dimensional dense granular sediments [18,19].

Recently, it was applied to follow an intruder sinking in a water-saturated dense granular suspension (akin to a Stokes viscometer) [20]. In that case, since the size of the grains was smaller than the wavelength of the ultrasound, a coherent echo from the intruder could be obtained from one packing configuration measurement using a standard single-element ultrasonic transducer (unfocused). Here we investigate another situation in which the grain size is close to the ultrasonic wavelength and scattering phenomena dominate wave propagation, leading to multiply scattered ultrasound (coda waves) [21,22] also known as material or structural noise in nondestructive evaluation of materials [23–25]. The intruder is located deeply inside such opaque granular sediment at a depth Z (approximately $20l^*$) much larger than the mean-free path of ultrasonic transport l^* (see below).

As a reminder, sound propagation through suspensions comprised of solid particles and a viscous fluid is in itself a problem of immense practical relevance because of its utility for seismic investigations and nonintrusive probes of materials such as ultrasonic spectroscopy [26]. The principle relies on measurements of the velocity and

*siet.van_den_wildenberg@uca.fr

†xiaoping.jia@espci.fr

attenuation of coherent ultrasonic waves propagating through the system. The interaction of ultrasound with the material depends on the contrast between the constituent components, the size distribution and the concentration of particles ϕ_s [27,28]. For the low particle concentrations ($\phi_s < 15\%$), two different methods have been particularly developed to determine the effective wave number of the coherent wave propagating in suspensions [29]: the coupled phase theory based on the two-phase hydrodynamic equations and the multiple scattering theory (also called ECAH theory [30,31]), which provide similar results in the low-frequency range or long wavelength regime, $\lambda \gg d$ with d the mean particle size [28]. For suspensions with high particle concentration ($\phi_s > 40\%$), the scattering mean-free path decreases significantly, leading to a large attenuation of the coherent ballistic waves even in the absence of absorption, and a dominant multiply scattered waves in transmitted ultrasonic signals. Moreover, in the intermediate frequency regime for $\lambda \sim d$, resonant scattering may occur, leading to a large dispersion of the wave velocity [32,33]. In this case, it is necessary to use the more general scattering theories, such as the coherent potential approximation (CPA) to determine the effective wave number of the coherent waves [26].

In this work, unlike the beam-forming technique where the multiple element ultrasonic transducer (array) is used to create different wave paths (configurations) between emissions and receptions via the target (intruder) [15–17], we use the single-element ultrasonic transducer for emission and reception but apply a configuration averaging process to extract the enhanced coherent echo from an intruder submerged in a dense granular suspension. Different configurations of the granular packing are realized by the nonaffine (random) motion of grains (scatters) induced continuously by a mixing blade situated at a certain distance away from the intruder. Similarly, diffusing wave spectroscopy (DWS) measurements employ an average over configurations of the scatter positions (e.g., colloidal particles), which allows the characterization of the random particle motion generated thermally or by fluidized beds [34,35]. But these two methods fundamentally differ in the averaging quantity, namely, the wave intensity in optics and the wave field in acoustics. We show that our configuration averaging of ultrasonic signals leads to a decrease or cancellation of incoherent scattered waves. The effects of the blade rotation speed and the blade-intruder distance is discussed in terms of grain motions (mean flow and nonaffine motion), observed in the wide shear zone of a split-bottom shear cell [36].

II. EXPERIMENT

Our setup consists of a glass container with diameter $D_c \sim 22$ cm filled with glass beads of diameter $d \sim$ 425–850 μm saturated by water up to $H \sim 6$ cm (Fig. 1).

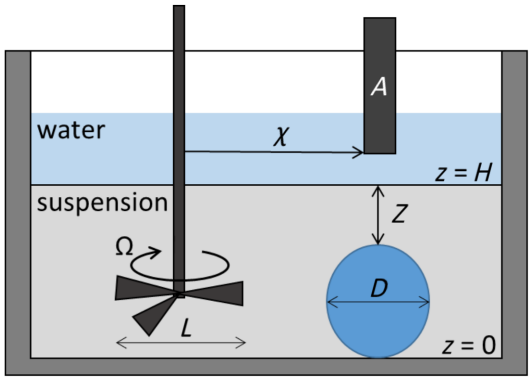

FIG. 1. Schematic of the experimental setup. A ball with a diameter of $D = 3$ cm is submerged at depth Z in a suspension of glass beads ($d \sim$ 425–850 μm) in water. A piezoelectric transducer (A) is used to send short pulses and measure the echoes from the interface and the surface of the ball. The scatter configuration in the granular packing may by modified by a mixing blade with size $L = 5$ cm and rotation speed Ω placed at a distance χ from the ball.

The gravitational sedimentation results in a dense granular suspension with initial packing density of about $\phi_s \sim 62\%$ calculated via $m/(\rho_p V)$ with m the mass of the glass beads, ρ_p the density of glass and V the volume occupied by the bead packing. To explore different configurations of the granular packing we use a mixing blade with a diameter $L \sim 50$ mm rotating at a velocity Ω. Under shear flow, ϕ_s is expected to decrease due to the dilatancy effect. A steel ball of diameter of $D = 30$ mm is placed at the bottom of the densely packed suspension at a distance χ from the rotating blade. The height of the suspension above the intruder is $Z \sim 15$ mm. Occasionally, the onset of rotation leads to a small change in the arrival of the echo from the interface of the suspension, suggesting there is a small dilation of the dense granular suspension. After this occasional initial dilation, we do not observe any significant change in the arrival of the first echo.

In order to determine the location of the intruder, a broadband transducer centred at $f_c = 2.25$ MHz is placed exactly above the intruder. The transducer emits short pulses and detect the echoes at a repetition rate approximately 256 Hz. An acoustic signal is obtained by averaging 512 pulses, which takes about 2 s, and an experiment consists of taking N (from 2 to 100) of such signals. The final acoustic trace is calculated by averaging these N signals. The associated wavelength of the ultrasound is $\lambda = c_w/f_c \sim 670$ μm with $c_w = 1500$ m/s the sound velocity in water (which is a bit smaller than the coherent longitudinal wave velocity $c_p \sim 1600$ m/s [32]). This is smaller than the intruder size and similar to the size of the glass beads ($d \sim \lambda \ll D$). Previous works on ultrasound propagation in a comparable dense granular suspension reported a transport mean-free path $l^* \sim d$ (∼0.5 mm) [22,37]. This

would correspond to a ratio $Z/l^* \sim 30$, suggesting strongly dominant scattering in our sample. Nevertheless, because of the high dissipation (the absorption time is as short as $\tau_a \sim 10\ \mu$s at $f \sim 2$ MHz [22]), the Anderson localization is not expected here.

III. RESULTS

To reduce the influence of ultrasound scattering ("material noise") and enhance the coherent echo, we develop here an approach based on a configuration averaging of transmitted ultrasonic signals to localize an intruder in a dense granular suspension. For this purpose, we focus on the effects of the following: (i) the number of averaged configurations, (ii) the blade mixing speed, and, (iii) the blade-intruder distance.

A. Effect of the configuration number

We start by exploring the influence of the number of averaged configurations on the ultrasound localization of the intruder at a distance $\chi = 8$ cm from the blade. In the absence of rotation, we observe one echo reflected from the interface between water and the granular suspension [Fig. 2(a1), dashed arrow] [20]. There is a faint second echo, which comes from the surface of the intruder [Fig. 2(a1), black arrow]. However, this second echo is largely obscured by the strongly scattered waves. We see in later examples that the coherent echo from the intruder can be completely hidden by the scattered waves. A spectrogram evidences the relevance of the higher-frequency scattered waves at the arrival of the lower-frequency coherent echo from the intruder [Fig. 2(a2)]. We then start exploring different configurations of the glass-bead packing by rotating the blade at a speed $\Omega \sim 23$ rpm. To

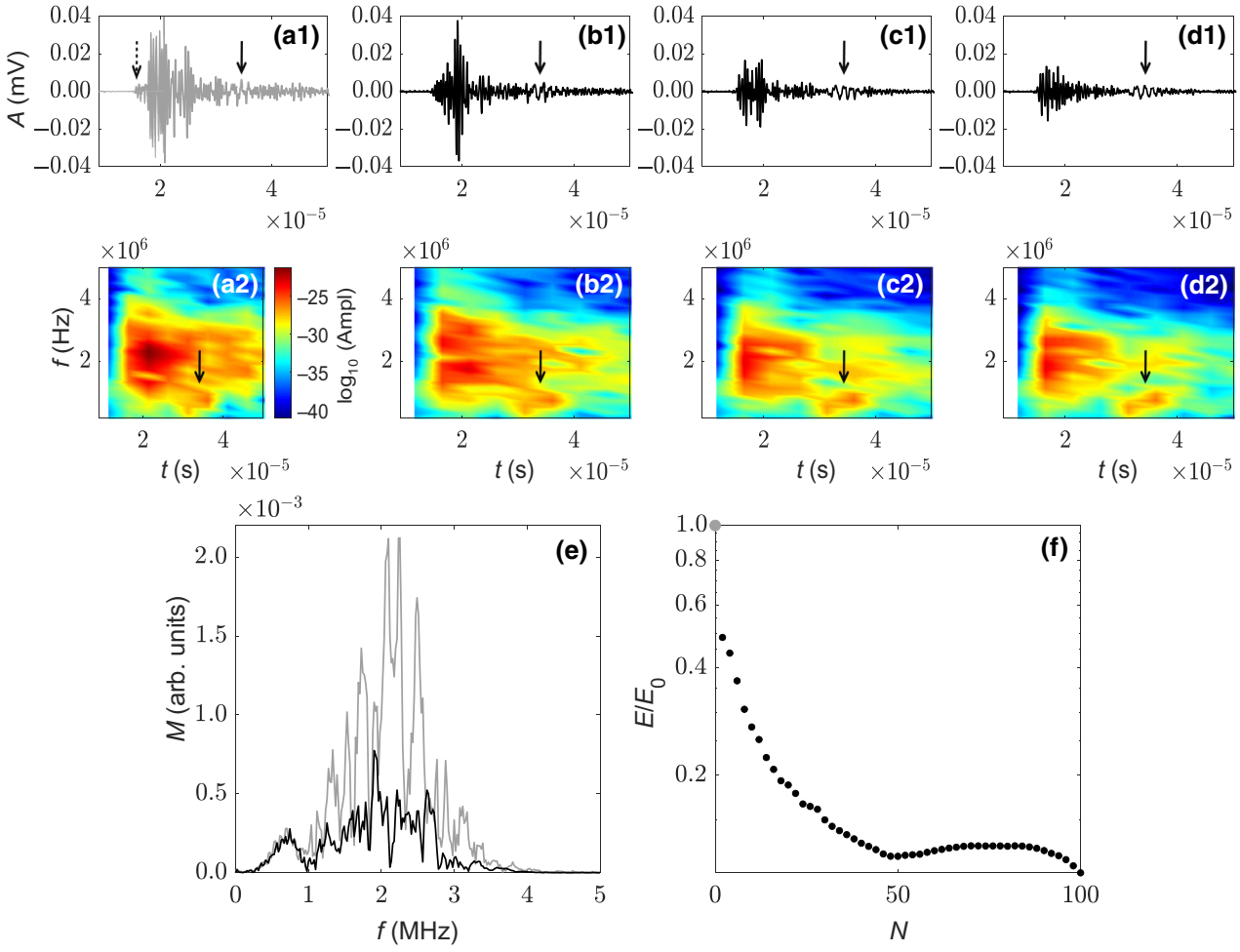

FIG. 2. Effect of configuration averaging for $\chi = 8$ cm. (a1) Acoustic signal obtained at $\Omega = 0$. (a2) Spectrogram of the acoustic signal in (a). (b1),(c1),(d1) Acoustic signals obtained for $\Omega = 23$ rpm and after averaging $N = 2$, 20 and 50 signals, respectively. (b2),(c2),(d2) Spectrograms of the signals in (b1),(c1),(d1). The coherent echo from the surface of the ball is indicated by the black arrow. The color indicates the log amplitude. (e) Power spectrum of the signals in (a1),(d1) in gray and black, respectively. (f) The energy of the propagating wave normalized by the energy of the wave at $\Omega = 0$, versus the number N of signals averaged (semi-logarithmic plot).

investigate the influence of the configuration averaging, we measure N (= 100) acoustic signals.

Acoustic traces are then calculated for an increasing number of averaged signals (from $N = 2$ to 100) and, for each trace, the contribution of scattered waves is evaluated. We find that for increasing configuration averaging, the scattered waves decrease and, consequently, the coherent echo from the intruder becomes more visible [Figs. 2(b1)–2(d1)]. This effect is even more evident in the spectrograms, where the low frequency coherent echo becomes well separated in time from scattered waves [Figs. 2(b2)–2(d2)].

A Fourier transform of the signal at $\Omega = 0$ and 23 rpm ($N = 50$) shows a low-frequency peak at approximately 0.8 MHz (indicated by the black arrow), which does not depend on N. This corresponds to the coherent wave with $\lambda_{\mathrm{coh}} = c_w/0.8e6 \sim 1.9$ mm much larger than the bead size. The amplitudes of frequencies corresponding to scattered waves (>1 MHz) are clearly decreased due to the configuration averaging [Fig. 2(e)].

In order to quantify the contribution of scattered waves to the acoustic trace, we calculate the total energy of the acoustic trace via $E = \int A(t)^2 dt$, here $A(t)$ is the (averaged) acoustic trace. The ratio of the energies is obtained through normalization by the energy of the acoustic trace E_0 at $\Omega = 0$. We find that the normalized energies first decrease rapidly with increasing the number of averaged signals. After $N \sim 50$ signals the normalized energy appears to reach a plateau, suggesting that nearly all the energy comes from the coherent echoes from the water-suspension interface and the intruder, and there is no further improvement of the signal by additional averaging [Fig. 2(e)].

B. Effect of the rotation speed

To explore the role of the rotation speed on scattered waves, we set the distance between the blade and the intruder and vary the rotation speed of the blade Ω from 20 to 154 rpm. For each Ω an acoustic trace is obtained by averaging $N = 100$ acoustic signals.

For $\chi = 7$ cm, we find that the contribution of scattered waves rapidly decreases with increasing Ω, as can be observed from the time traces and the spectrograms [Fig. 3(a)–3(d)]. Indeed, for $\Omega = 62$ rpm, there is a clear separation in time and frequency of scattered waves and the coherent echo from the intruder. Instead, if the distance between the rotating blade and the intruder is larger, at $\chi =$ 9.5 cm, the visibility of the coherent echo from the intruder appears to arrive at higher $\Omega \sim 119$ rpm [Figs. 3(e)–3(h)].

To further quantify the effect of the rotation speed, we calculate again the normalized energy and show it as a function of the rotation speed in Fig. 3(i). When the distance between the rotating blade and the intruder is small, the energy of the acoustic signal rapidly decreases to its plateau value corresponding to the energy of the coherent echo. For larger distance to the rotating blade, the decrease of the contribution of scattered waves to the energy appears more gradual.

C. Effect of the blade-intruder distance

Next, the effect of the distance between the intruder and the rotating blade χ for $\Omega = 40$ rpm is investigated. To this end, χ is varied between 7, 8.2, 9.5, and ll cm and for each χ the acoustic trace is obtained by averaging $N = 100$ signals and E is calculated (Fig. 4). We find that the contribution of scattered waves increases rapidly with increasing χ resulting in less visibility of the coherent echo at large χ. Indeed at $\chi = 11$ cm, the coherent echo is hidden by scattered waves showing the relevance of the distance to the sheared zone.

IV. DISCUSSION

A. Independent configurations in sheared granular packings

We address the challenge of localizing an intruder in a strong ultrasound scattering medium, such as a dense granular suspension, by the use of configuration averaging. We show that there are, at least, three manners to decrease scattered waves: (i) increasing the number of configurations averaged, or (ii) increasing the mixing speed, or (ii) decreasing the blade-intruder distance.

The question is then what is the relevant parameter to determine the independent configurations? To answer this question, we calculate the time necessary to obtain independent configurations induced by rotational shear flow. For this, we return to the data shown in Fig. 2 at $\chi = 8$ cm and $\Omega = 23$ rpm, and determine the acoustic traces by averaging two acoustic signals ($N = 2$) separated by a lag time δt. Subsequently, we calculate for each acoustic trace the energy E and then average the E's for a given δt so as to obtain $\langle E \rangle$, and the ratio $\langle E \rangle / E_0$ is evaluated as a function of δt (Fig. 5). For increasing lag time, we find that the normalized energy first decreases rapidly to approximately 0.3 at δt^*, and then remains nearly constant [Fig. 5(a)]. The minimal time lag to randomize the scattering waves is $\delta t^* \sim 30$ s corresponding to about 12 rotations, and more rotations do not yield an improved cancellation of scattered waves. Note that the value for the normalized energy (approximately 0.3) at δt^* is higher than the minimal value obtained by configuration averaging (approximately 0.1) in Fig. 2 where a larger number of independent configuration are involved for averaging $\Delta t/\delta t^*$ (greater than six with the recording time $\Delta t \sim 200$ s) even though all N configurations used are not completely independent.

Moreover, we repeat the procedure for the data obtained at $\chi = 7$ cm with different Ω (corresponding to the data shown in Fig. 3). The ratio $\langle E \rangle / E_0$ versus δt decreases with

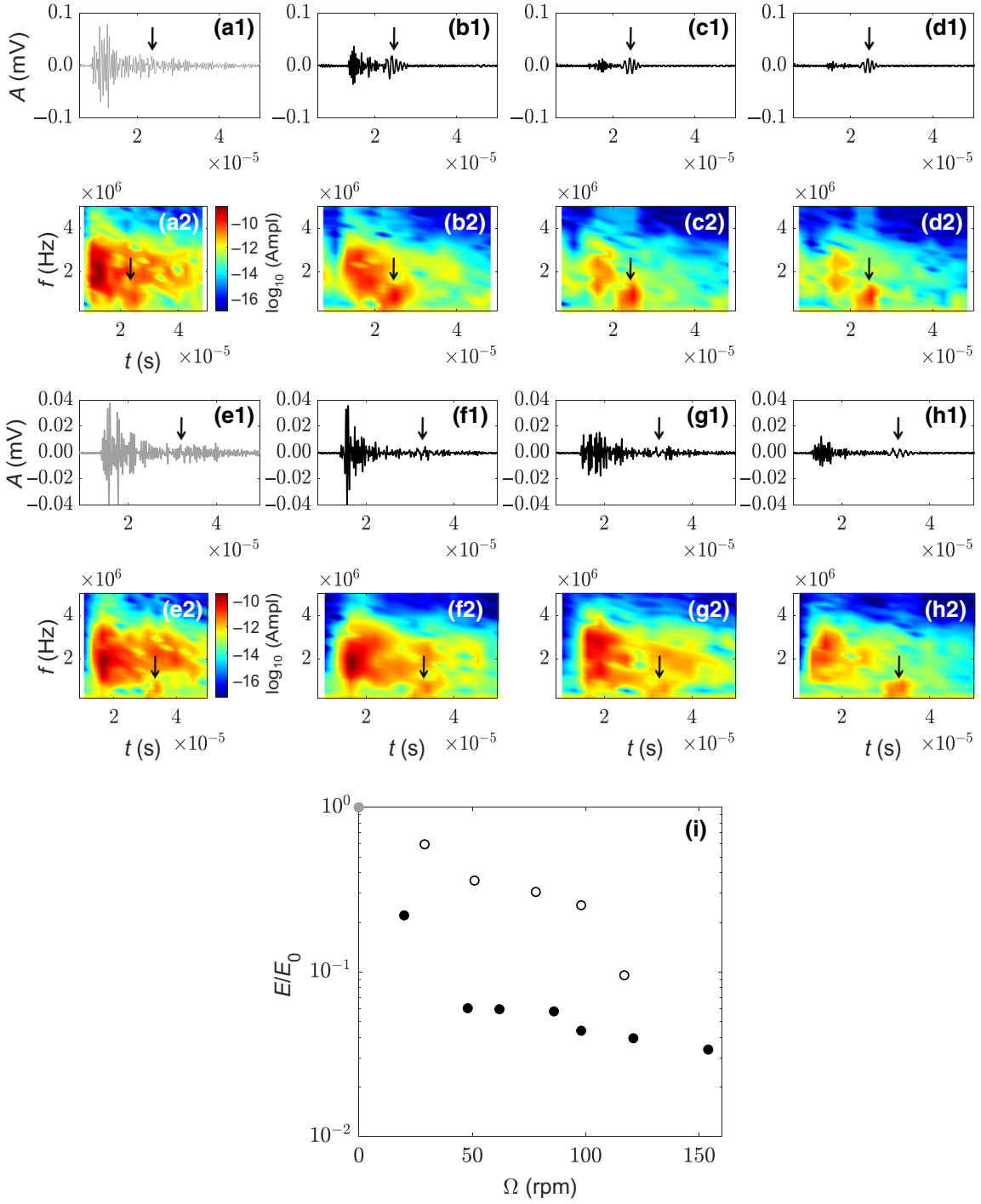

FIG. 3. Effect of the rotation speed of the blade observed at $\chi = 7$ and 9.5 cm, respectively. (a1) Acoustic signal obtained for $\Omega = 0$ at $\chi = 7$ cm. (b1),(c1),(d1) Acoustic signals at $\chi = 7$ cm for $\Omega = 20$, 62, 121 rpm. (a2),(b2),(c2),(d2) Spectrograms of the signals in (a1),(b1),(c1),(d1). (e1) Acoustic signal obtained for $\Omega = 0$ at $\chi = 9.5$ cm. (f1),(g1),(h1) Acoustic signals at $\chi = 9.5$ cm for $\Omega = 22$, 75, 119 rpm. (e2),(f2),(g2),(h2) Spectrograms of the signals in (e1),(f1),(g1),(h1). The coherent echo from the surface of the ball is indicated by the black arrow. (i) The energy of the transmitted wave normalized by the wave energy for $\Omega = 0$ is plotted versus the rotation speed, showing a clear decrease with increasing Ω. Solid points are $\chi = 7$ cm, open circles are $\chi = 9.5$ cm.

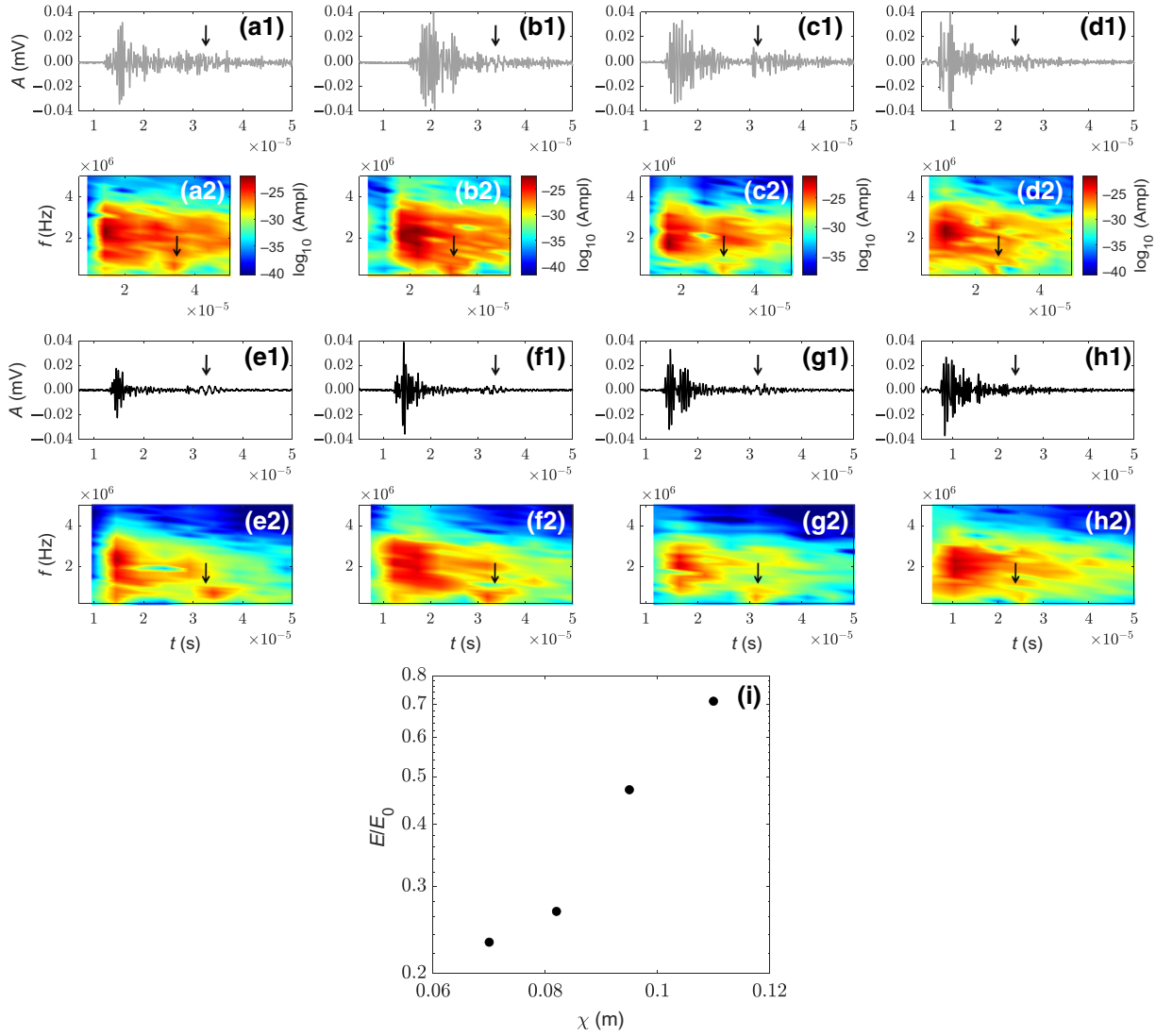

FIG. 4. Effect of the blade-intruder distance. (a1) Trace at $\chi = 7$ cm for $\Omega = 0$ rpm with its spectrogram in (a2). (b1) Trace at $\chi = 8.2$ cm for $\Omega = 0$ rpm with its spectrogram in (b2). (c1) trace at $\chi = 9.5$ cm for $\Omega = 0$ rpm with its spectrogram in (c2). (d1) Trace at $\chi = 11$ cm for $\Omega = 0$ rpm with its spectrogram in (d2). (e1) Trace at $\chi = 7$ cm for $\Omega = 40$ rpm with its spectrogram in (e2). (f1) Trace at $\chi = 8.2$ cm for $\Omega = 40$ rpm with its spectrogram in (f2). (g1) Trace at $\chi = 9.5$ cm for $\Omega = 40$ rpm with its spectrogram (g2). (h1) Trace at $\chi = 11$ cm for $\Omega = 40$ rpm with its spectrogram in (h2). The coherent echo from the ball is indicated by the black arrow. (i) The energy ratio of the averaged acoustic trace to the signal obtained for $\Omega = 0$ versus the blade-intruder distance. This energy ratio increases with increasing χ, suggesting that the averaging process becomes less efficient further from the shear zone.

increasing Ω [Fig. 5(b)], showing that at higher Ω independent configurations are more rapidly obtained. From Fig. 5, we estimate $\delta t^* \sim 30$, 10, and 5 s for $\Omega = 20$, 62, and 121 rpm, respectively. In these experiments at $\chi = 7$ cm, independent configurations are thus obtained after about ten rotations.

B. Grain motions and contact network changes

In order to investigate the flow of the granular suspension (immersed glass beads) sheared by our mixing blade [Figs. 6(a) and 6(b)], we film the surface of the suspension added with a few white ceramic beads of $d \sim 1$ mm (kind of "tracers") for $\Omega = 31$, 68, 95, and 120 rpm. To identify qualitatively the sheared zone we first make an image from the superposition (averaging) of all the frames in a movie (approximately 6000) at a given Ω. The texture of such images is partly blurred in the region where there is motion of the glass particles (and tracer particles) [Figs. 6(c)–6(f)]. The blurring in the image is quantified by calculating a local standard deviation of the pixel intensity $\sigma_L \sim 0$ from the standard deviation of the 3-by-3

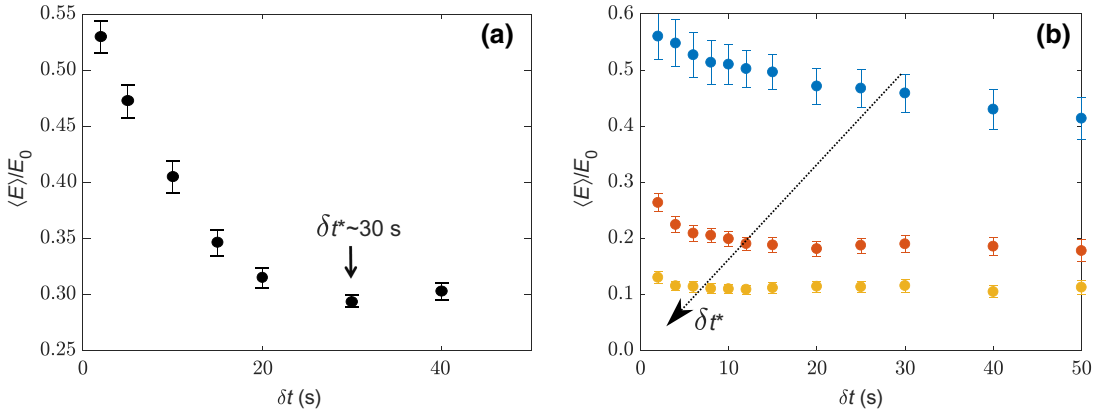

FIG. 5. Time necessary to randomize the scattering waves. (a) Normalized energy calculated from the data in Fig. 2 ($\chi = 8$ cm and $\Omega = 23$ rpm) by averaging two signals ($N = 2$) for increasing time lag between them. To completely randomize the scattering waves $\delta t^* \sim 30$ s. (b) The normalized energy of the wave versus the delay time for $\Omega = 20$, 62, and 121 rpm (blue, red, and yellow, respectively) at a distance $\chi = 7$ cm calculated from the data in Fig. 3. The dotted arrow indicates the decrease of δt^* with increasing Ω. Error bars represent the standard error of the mean.

neighborhood around each pixel, and averaging over all the pixels along the y direction. Smoothing or blurring results in low values of σ_L. Instead, the texture of the image where the particles are static results in a high value of $\sigma_L \sim 1$. To qualitatively illustrate the size of the sheared zone (and its increase with Ω), we indicate the location at which $\sigma_L = 0.9$ in Figs. 6(c)–6(g).

A detailed investigation of the shear induced flow in the dense granular suspension is beyond the scope of this paper. Instead, we seek to analyze our results within

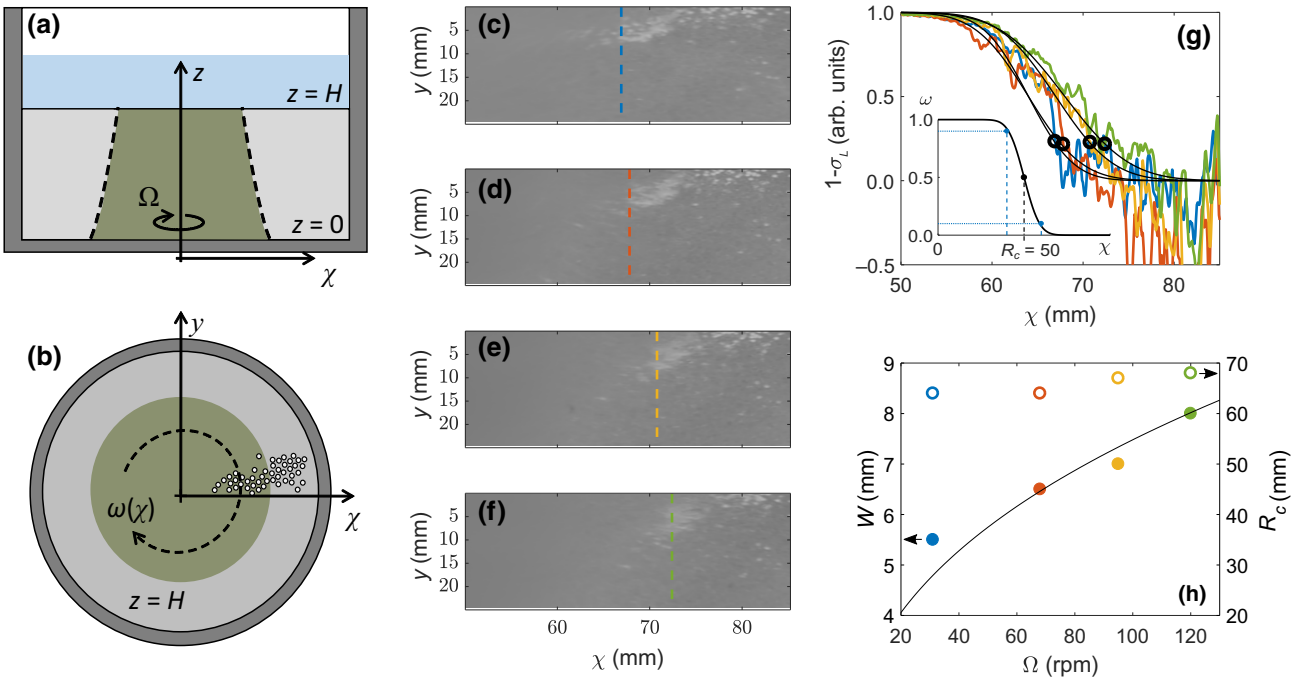

FIG. 6. (a) Sketch of side view and (b) top view of the shear zone (in green) induced by the mixing blade (split-bottom-like shear cell). The location of tracer beads is indicated (right) for illustration. (c)–(f) Images obtained from averaging 6000 frames from a movie (about 100 s) at rotating speeds $\Omega = 31$, 68, 95, 120 rpm, respectively. The texture of the image is smoothed due to the particle motion by shear. The dotted lines are a guide to the eye, they indicate χ for which $\sigma_L = 0.9$ and illustrate the increase of the flowing zone with Ω. (g) $(1 - \sigma_L)$ as a function of χ for the images in (c)–(f) colors blue, red, yellow, and green are $\Omega = 31$, 68, 95, 120 rpm, respectively. Open circles depict $\sigma_L = 0.75$. The black lines are models of $\omega(\chi)$ obtained from Eq. (1) by setting R_c and W. Inset shows a typical trace of $\omega(\chi)$ with $R_c = 50$ mm and $W = 10$ mm. (h) The W (points) and R_c (circles) used for the models in (f) versus Ω. The black line corresponds to a power law $W \sim \Omega^{0.38}$ [39].

a rheological model developed for dry granular media in a split-bottom shear cell [11,38,39]. Even though the driving geometries differ, the relatively wide shear zone we observe in our device is expected to be reminiscent to those observed in split-bottom geometries for shallow granular layers [Figs. 6(a) and 6(b)]. Furthermore, the flow appears to be nearly stationary, i.e., the sheared region does not change much in time [38]. We thus describe ω, the dimensionless ratio between the observed (average) angular velocity of the surface particles and Ω, as a function of the distance from the rotating blade χ via [38,39]

$$\omega(\chi) = (1/2) - (1/2)\mathrm{erf}[(\chi - R_c)/W], \qquad (1)$$

where R_c and W denote the center position and width of the shear band, respectively [see the inset in Fig. 6(g)]. We assume that the texture in the images is correlated to ω as $\omega \sim (1 - \sigma_L)$. This appears reasonable since $\omega \sim 1$ would results in $\sigma_L \to 0$, while $\omega \sim 0$ would yield in $\sigma_L \to 1$ [Fig. 6(g)]. Therefore, the experimental data of $(1 - \sigma_L)$ versus χ for the different Ω is modeled by Eq. (1) using R_c and W as fit parameters. We find that this rheological model qualitatively describes our data for different Ω [Fig. 6(g)]. The deduced R_c and W are shown as a function of Ω in Fig. 6(h). The observed dependence of W on Ω is close to the expected power-law increase [39], whereas R_c increases only slightly (<5%) with Ω. The increase of W with Ω results in particles with a higher ω, at a given χ, explaining the improved cancellation of scattered waves observed for higher Ω (see below).

Of note, the experiments in which $\chi > R_c + W \sim 70$ mm evidenced that cancellation of scattered waves can be obtained even outside the mean flowing zone where no visible particle motion is observed. This phenomenon may be related to the contact network change of the granular packing arising from the microslips between grains induced by shear, which has been evidenced by the decorrelation of the multiply scattered ultrasound through the changing contact network (from grain to grain) under shear [40]. Such nonlocal rheological behavior is consistent with what can be observed in fluidlike quiescent regions far away from the main flow generated by a localized slow stirring or a shear band [41,42]. The creep velocity of the local probe may vary with the distance to the shear band and nonaffine motions of grain could be described by Eyring-like activation process (via effective temperature) [42]. Further investigation on this issue is still needed in the future.

For $\Omega = 31$ rpm, $W = 5.5$ mm, and $R_c = 64$ mm, the angular velocity in the tail of the shear band ($\chi = 80$ mm) is $\omega \sim 1 \times 10^{-4}$ rpm, which corresponds to a linear velocity of $v \sim 0.01$ mm/s. Considering v and the minimal delay to randomize scattered waves $\delta t^* = 30$ s, this suggests that the cumulative displacement (including both the coherent and incoherent parts) of the beads is approximately 0.15 mm. The cumulative displacement is thus comparable to half wavelength of ultrasound ($\lambda/2 \sim 0.33$ mm), leading to the destructive interference between scattered waves traveling through nearly independent configurations of the packing and consequently their reduction or cancellation. The observation that δt^* decreases with increasing Ω qualitatively agrees with the picture that there exists a critical displacement $u_c \sim \lambda/2$ necessary in order to obtain optimal cancellation of scattered waves.

We are aware that the estimations proposed here are rough and further investigation is needed in the future to better quantify the rheological behavior in dense granular suspensions. In particular, the above split-bottom shear model is originally developed for dry granular media in which the effects associated with liquid pore pressure are neglected. This may be illustrated by considering that the ratio $H/R_s \sim 1.8$, with $H \sim 45$ mm and $R_s \sim L/2 = 25$ mm. Typically, for such values of H/R_s, flows do not reach the surface of the suspension [38,39]. However, we clearly observe surface flow, suggesting an effective R_s^* larger than R_s, likely due to the effects of pore fluid pressure. In particular, the migration effect may be significant when there is a gradient in the flow velocity, which may lead to hydrodynamic lubrication between different sheared layers.

Despite this limitation, the model appears to capture reasonably well our observations of the sheared region. Moreover, the inferred estimations support the idea that configuration averaging results in cancellation of scattered waves due to microscopic rearrangements of grains (microslips at the contact level), leading to the contact network change without visible macroscopic rearrangements of grains [41,42].

V. CONCLUSION

We demonstrate the applicability of a standard single-element ultrasonic transducer to localize an intruder in a highly scattering dense granular suspension via a configuration-averaging process. Our results show that multiply scattered ultrasound, considered as the material noise, can be significantly reduced by averaging the acoustic signals over the changed granular packing in a wide shear zone induced by a distant mixing blade, enhancing thus the visibility of the coherent echo from the intruder. Furthermore, increasing the shear speed or/and decreasing the distance between the shearing blade and the intruder results in a decrease of scattered waves, which is consistent with the shear zone observed in a split-bottom rotating shear cell.

We believe that the acoustic method developed in this work may provide a practical tool for localizing buried objects in dense turbid marine sediments. It also paves the way for a nonlocal rheology to monitor the ball falling in a sheared or vibrated dense granular suspension with

the acoustic tracking [20,41], which allows a better understanding of quicksands and liquefaction phenomena.

ACKNOWLEDGMENT

This work has received support under the program "Investissements d'Avenir" launched by the French Government. S.W. also acknowledges support by Clervolc Contribution No. 575.

[1] P. Coussot, *Rheometry of Pastes, Suspensions and Granular Materials* (Wiley, New York, 2005).
[2] B. Andreotti, Y. Forterre, and O. Pouliquen, *Granular Media: Between Fluid and Solid* (Cambridge University Press, Cambridge, 2013).
[3] A. J. Liu and S. R. Nagel, *Jamming and Rheology* (Taylor & Francis, New York, 2001).
[4] A. Fall, H. de Cagny, D. Bonn, G. Ovarlez, E. Wandersman, J. Dijksman, and M. van Hecke, Rheology of sedimenting particle pastes, J. Rheol. (N. Y.) **57**, 1237 (2013).
[5] F. Boyer, E. Guazzelli, and O. Pouliquen, Unifying Suspension and Granular Rheology, Phys. Rev. Lett. **107**, 188301 (2011).
[6] G. MiDi, On dense granular flows, Eur. Phys. J. E **14**, 341 (2004).
[7] S. Courrech du Ponts, P. Gondret, B. Perring, and M. Rabaud, Granular Avalanches in Fluids, Phys. Rev. Lett. **90**, 044301 (2003).
[8] C. Cassar, M. Nicolas, and O. Pouliquen, Submarine granular flows down inclined planes, Phys. Fluids **17**, 10331 (2005).
[9] K. Kamrin and G. Koval, Nonlocal Constitutive Relation for Steady Granular Flow, Phys. Rev. Lett. **108**, 178301 (2012).
[10] H. Jaeger, S. Nagel, and R. Behringer, Granular solids, liquids, and gases, Rev. Mod. Phys. **68**, 1259 (1996).
[11] P. Shall and M. van Hecke, Shear bands in matter with granularity, Annu. Rev. Fluid. Mech. **42**, 67 (2010).
[12] S. Manneville, Recent experimental probes of shear banding, Rheol. Acta. **47**, 301 (2008).
[13] M. Liberatore, F. Nettesheim, N. Wagner, and L. Porcar, Spatially resolved small-angle neutron scattering in the 1–2 plane: A study of shearinduced phase-separating wormlike micelles, Phys. Rev. E **73**, 020504 (2006).
[14] P. Callaghan, Rheo NMR and shear banding, Rheol. Acta **47**, 243 (2008).
[15] T. Gallot, C. Perge, V. Grenard, M. A. Fardin, N. Taberlet, and S. Manneville, Ultrafast ultrasonic imaging coupled to rheometry: Principle and illustration, Rev. Sci. Instrum. **84**, 045107 (2013).
[16] B. Saint-Michel, H. Bodiguel, S. Meeker, and S. Manneville, Simultaneous Concentration and Velocity Maps in Particle Suspensions under Shear from Rheo-Ultrasonic Imaging, Phys. Rev. Appl. **8**, 014023 (2017).
[17] J. Brum, J. Gennisson, M. Fink, A. Tourin, and X. Jia, Drastic slowdown of the Rayleigh-like wave in unjammed granular suspensions, Phys. Rev. E **99**, 042902 (2019).
[18] S. Swaminathan, D. Visco, and S. Sen, Detection of shallow inclusion in closed-packed granular beds using mechanical impulses, Appl. Phys. Lett. **90**, 154107 (2007).
[19] E. Han, N. van Ha, and H. M. Jaeger, Measuring the porosity and compressibility of liquid-suspended porous particles using ultrasound, Soft Matter **13**, 3506 (2017).
[20] S. van den Wildenberg, X. Jia, J. Léopoldès, and A. Tourin, Ultrasonic tracking of a sinking ball in a vibrated dense granular suspension, Sci. Rep. **9**, 5460 (2019).
[21] A. Tourin, A. Derode, and M. Fink, Multiple scattering of sound, Waves Random Media **10**, 345 (2000).
[22] J. Page, H. Schriemer, A. Bailey, and D. Weitz, Experimental test of the diffusion approximation for multiply scattered sound, Phys. Rev. E **52**, 3 (1995).
[23] L. Ericsson and T. Stepinski, in *Review of Progress in Quantitative Nondestructive Evaluation: Volumes 12A and 12B*, edited by D. O. Thompson and D. E. Chimenti (Springer US, Boston, MA, 1993), p. 695.
[24] E. Larose, A. Derode, M. Campillo, and M. Fink, Imaging from one-bit correlation of wideband diffusive wave fields, J. Appl. Phys. **95**, 8393 (2004).
[25] S. Shahjahana, F. Rupina, T. Fouquetb, A. Aubryc, and A. Derodec, in *Proceedings of the Acoustics 2012 Nantes Conference* (Nantes, France, 2012), Vol. 2645.
[26] P. Sheng, *Introduction to Wave Scattering, Localization and Mesoscopic Phenomena* (Springer, Berlin, 2006).
[27] V. Stolojanu and A. Prakash, Characterization of slurry system by ultrasonic techniques, Chem. Eng. J. **84**, 215 (2001).
[28] R. Challis, M. Povey, M. Mather, and A. Holmes, Ultrasound technique for characterizing colloidal dispersions, Rep. Prog. Phys. **68**, 1541 (2005).
[29] T. Valier-Brasier, J.-M. Conoir, F. Coulouvrat, and J.-L. Thomas, Sound propagation in dilute suspensions of spheres: Analytical comparison between coupled phase model and multiple scattering theory, J. Acoust. Soc. Am. **138**, 2598 (2015).
[30] J. R. Allegra and S. A. Hawley, Attenuation of sound in suspensions and emulsions: Theory and experiments, J. Acoust. Soc. Am. **51**, 1545 (1972).
[31] P. S. Epstein and R. R. Carhart, The absorption of sound in suspensions and emulsions. I. Waterfog in air, J. Acoust. Soc. Am. **25**, 553 (1953).
[32] H. Schriemer, M. Cowan, J. Page, P. Sheng, Z. Liu, and W. D. A., Energy Velocity of Diffusing Waves in Strongly Scattering Media, Phys. Rev. Lett. **79**, 3166 (1997).
[33] B. Tallon, T. Brunet, J. Leng, and J. Page, Energy velocity of multiply scattered waves in strongly scattering media, Phys. Rev. B **101**, 054202 (2020).
[34] D. J. Pine, D. A. Weitz, G. Maret, P. E. Wolf, E. Herbolzheimer, P. M. Chaikin, and P. Sheng, in *Scattering and Localization of Classical Waves in Random Media*, edited by P. Sheng (World Scientific, Singapore, Singapore, 1990).
[35] M. Cowan, I. Jones, J. Page, and D. Weitz, Diffusing acoustic wave spectroscopy, Phys. Rev. E **65**, 06605 (2002).

[36] J. A. Dijksman and M. van Hecke, Granular flows in split-bottom geometries, Soft Matter **6**, 2901 (2010).
[37] M. Harazi, Ph.D Thesis, Universitè de Paris Diderot (in French), Paris, 2017.
[38] D. Fenistein, J. van de Meent, and M. van Hecke, Universal and Wide Shear Zones in Granular Bulk Flow, Phys. Rev. Lett. **92**, 094301 (2004).
[39] P. Jop, Hydrodynamic modeling of granular flows in a modified couette cell, Phys. Rev. E **77**, 032301 (2008).
[40] Y. Khidas and X. Jia, Probing the shear-band formation in granular media with sound waves, Phys. Rev. E **85**, 051302 (2012).
[41] K. Nichol, A. Zanin, R. Bastien, E. Wandersman, and M. van Hecke, Flow-Induced Agitations Create a Granular Fluid, Phys. Rev. Lett. **104**, 48 (2010).
[42] K. Reddy, Y. Forterre, and O. Pouliquen, Evidence of Mechanically Activated Processes in Slow Granular Flows, Phys. Rev. Lett. **106**, 108301 (2011).